Magneto-optical Kerr spectroscopy of platinum

L. Uba,* S. Uba, and V. N. Antonov†
Institute of Experimental Physics, University of Bialystok, Lipowa 41, PL-15-424 Bialystok, Poland

A. N. Yaresko†
Max-Planck-Institut for the Physics of Complex Systems, D-01187 Dresden, Germany

R. Gontarz
Institute of Molecular Physics, Polish Academy of Sciences, Smoluchowskiego 17, PL-60-179 Poznan, Poland
(Received 16 June 2000; revised manuscript received 21 September 2000)

Magneto-optical (MO) response of paramagnetic Pt is reported. The magneto-optical polar Kerr effect spectra of the paramagnetic fcc Pt metal film were measured with high sensitivity in an applied magnetic field of 1.5 T over the photon energy range 0.74–5.6 eV. It is shown that the *ab initio* linear muffin-tin orbital (LMTO) calculations reproduce the experimental spectra well and allow us to explain the microscopic origin of the Pt magneto-optical response in terms of interband transitions. The importance of the off-diagonal intraband Drude-like transitions is demonstrated explicitly and found to be the predominant contribution to the observed spectra in the ir range. The band-by-band decomposition of the fcc Pt MO spectra is presented and the interband transitions responsible for the prominent structures in the spectra are identified. The contributions coming from the vicinity of high-symmetry points of the Brillouin zone are quantitatively determined. A comparative study of the relation between the main spectral features in the Pt and Pd metals and the peculiarities of their band structures is performed. It is shown that the individual interband transitions arising from the same points of **k** space characterize essentially similar spectral shapes in both metals, but due to different energy locations they result in different optical and MO spectra. The influence of the magnetic field and spin-orbit coupling on the MO interband transitions in Pt is discussed. The crucial role of the transitions involving the states near the Fermi level is elucidated.

I. INTRODUCTION

The electronic structure of Pt and Pd metals was extensively studied both experimentally[1–4] and theoretically[5–12] as long as 15–30 years ago. It is not possible to mention all publications on this subject in a short introduction. From the very good agreement between various theoretical band-structure calculations and a great variety of the experimental measurements, it can be concluded that the electronic structures of Pt and Pd are known in great detail.

In the past decade, interest in Pt and Pd metals has greatly increased again due to outstanding physical properties of their compounds.[13–18] In particular, (Co,Fe)–(Pt,Pd) alloy films as well as related multilayered structures exhibit perpendicular magnetization and a large magneto-optical Kerr rotation in the uv spectral range simultaneously.[13–15,17] Such a combination of properties together with their high chemical stability make these materials promising candidates for high-density magneto-optical recording media in the new generation of storage devices.[13] The underlying mechanism of the unique magnetic and magneto-optical properties of these systems has been ascribed to the well known ability of transition metals to induce a large spin polarization of Pt and Pd via strong $3d$-$(4d,5d)$ hybridization and exchange interaction at the (Co,Fe)/(Pd,Pt) interfaces in the layered structures[16,17] as well as in the vicinity of the magnetic impurities in the diluted alloys.[18]

On the other hand, Pt and Pd are closely related metals and are very interesting themselves. The shapes of the Fermi surfaces of Pt and Pd are found to be remarkably similar. Each metal has a closed electron surface centered around Γ, a small-volume closed-hole surface centered around X, and a large-volume open-hole surface (the ''jungle gym'') also centered around the X point.[1,5] As can be expected from the band structures, many of the electronic properties of Pt and Pd are also very similar and possible differences can arise from the stronger influence of relativistic effects on the band structure of Pt metal. The unique properties of Pt and Pd stimulated a large number of experimental and theoretical investigations of their physical properties such as de Haas–van Alphen effect,[1] electrical resistivity,[6] lattice dynamics and thermodynamical properties,[7] optical properties,[2,10,11] point-contact spectra,[12] soft x-ray emission[3] and photoemission[4] spectra, electron-phonon interaction,[8] the gyromagnetic factor of conduction electrons,[9] and so on. To the best of our knowledge, the magneto-optical properties of Pt metal have not yet been investigated.

Magneto-optical phenomena reflect the electronic states of the spin-polarized band structure and arise from simultaneous occurrence of the exchange splitting and spin-orbit coupling. In particular, the magneto-optical Kerr effect (MOKE) spectroscopy is a useful tool for investigating the electronic structure of magnetic materials, being sufficiently sensitive to probe changes in a spin-polarized band structure. High sensitivity of the MOKE spectra to structural changes that are accompanied by substantial electronic structure changes was observed.[19,20]

A substantial amount of experimental and first principles

 ©2000 The American Physical Society

calculation studies[17,19,21–29] have been performed to gain an understanding of the microscopic origin of the large Kerr effect in magnetic $3d$ transition metal (TM)-Pt systems, and it is well established that the prime origin of the large Kerr rotation in TM–Pt compounds[21–23,26] and multilayers[24–28] is the spin-orbit coupling on Pt. As it was shown in Ref. 27 the origin of the strong enhancement of MOKE in the TM/Pt multilayers arises due to a strong hybridization between the Co,Fe($3d$) and Pt($5d$) orbitals, and as a result the spin polarization of the magnetic $3d$ atoms is transferred to the nonmagnetic Pt atoms and stronger spin-orbit coupling of the Pt atoms is transmitted to the $3d$ (Fe,Co) atoms.

The knowledge about the MO properties of pure Pt metal is very desirable and interesting itself and can be obtained by the direct measurement of the MOKE spectra of pure Pt metal combined with *ab initio* band-structure studies, which have been successfully applied to describe the MO properties of a wide class of ferromagnetic materials in the last few years (see, e.g., Ref. 29, and references therein). The MOKE spectra of paramagnetic fcc Pd metal have been investigated experimentally and theoretically in our previous paper.[30] It was shown that the main contribution to the formation of the MO response of Pd metal comes from the transitions from states in the vicinity of the Fermi level, and the spectra of strongly diluted Co-Pd and Fe-Pd alloys can be considered in a first approximation as the Kerr spectra of spin-polarized Pd.

This paper presents an original experimental and detailed theoretical investigation of the MO properties of pure Pt metal induced by an external magnetic field. From the detailed analysis of the interband transitions responsible for the Pt and Pd MOKE spectra, it has been found that in spite of the well known similarities of many electronic properties of Pt and Pd metals, the subtle differences of their electronic band structure result in the individual behavior of the MO response of these metals. To examine the dependence of the Pt MO properties on the source of Pt magnetization, we investigated the correlations between the magneto-optical response of paramagnetic Pt (where the magnetic moment on Pt is induced by an external magnetic field) and that of Pt in the dilute TM–Pt alloy (where the Pt magnetic moment arises as a result of hybridization with the magnetic $3d$ atoms).

The paper is organized as follows. The description of the experimental procedure and theoretical framework is provided in Sec. II. Section III presents the experimental and theoretical MO spectra of paramagnetic Pt in the external magnetic field. The theoretical analysis of the electronic structure and MO properties of Pt is presented in Sec. IV. Finally, the results are summarized in Sec. V.

II. EXPERIMENTAL AND THEORETICAL DETAILS

To study the magneto-optical response of Pt metal itself we measured the polar MOKE spectra of the paramagnetic Pt film in the external magnetic field of 1.5 T aligned normal to the film plane over the photon energy range $0.74 \leqslant \hbar\omega \leqslant 5.6$ eV. Thick ($\sim$2000 Å) polycrystalline fcc Pt films were prepared using a dc sputtering deposition system. The polar Kerr effect induced in Pt by the magnetic field of 1.5 T is very small (below 2×10^{-3} deg) and was detected in a sensitive Kerr spectrometer setup[26] by means of the polarization modulation technique using a piezobirefringent modulator. Besides the high sensitivity reaching the 10^{-5}–10^{-4} deg range (depending on the photon energy and corresponding photon shot noise), this method has the advantage that the Kerr rotation and Kerr ellipticity can be determined simultaneously. The resulting complex Kerr rotation values were determined to be half of the difference of the signals measured with the magnetic field of 1.5 T switched alternately between the positive and negative values. The acquisition time was long enough to obtain a sufficiently large signal-to-noise ratio. The precise calibration procedure of the Kerr rotation and ellipticity was performed before the measurements. The measurements were repeated a number of times on different samples and the resulting spectra presented in the paper were obtained by averaging over all the measurements. The optical properties were measured directly on the same samples by conventional spectroscopic ellipsometry using the rotating analyzer method over the same spectral range as that for the MOKE spectra.

Phenomenologically, magneto-optical effects at optical frequencies are treated by means of the optical conductivity tensor. In the polar geometry, where the z axis is chosen to be perpendicular to the solid surface and parallel to the magnetization direction, the expression for the complex Kerr angle is given by[31]

$$\theta_K(\omega)+i\varepsilon_K(\omega)=\frac{-\sigma_{xy}(\omega)}{\sigma_{xx}(\omega)\sqrt{1+(4\pi i/\omega)\sigma_{xx}(\omega)}}, \quad (1)$$

with θ_K the Kerr rotation and ε_K the Kerr ellipticity. $\sigma_{\alpha\beta}(\alpha,\beta\equiv x,y,z)$ is the optical conductivity tensor, which is related to the dielectric tensor $\varepsilon_{\alpha\beta}$ through

$$\varepsilon_{\alpha\beta}(\omega)=\delta_{\alpha\beta}+\frac{4\pi i}{\omega}\sigma_{\alpha\beta}(\omega). \quad (2)$$

Here and henceforth, the following definitions have been adopted. We choose the time dependence of the electric field as $\exp(-i\omega t)$. Hence, all the complex quantities are expressed by their real and imaginary parts as follows: $\sigma_{\alpha\beta}=\sigma^{(1)}_{\alpha\beta}+i\sigma^{(2)}_{\alpha\beta}$, $\varepsilon_{\alpha\beta}=\varepsilon^{(1)}_{\alpha\beta}+i\varepsilon^{(2)}_{\alpha\beta}$, where $\varepsilon_{xx}=(n+ik)^2$, and n and k are the refractive index and extinction coefficient, respectively.

The optical conductivity tensor components, or equivalently, the dielectric tensor components are the basic spectral quantities of the medium and can be evaluated from the optical and Kerr effect measurements.[32] The complex optical conductivity tensor components for the metals can be separated into two terms,

$$\sigma_{\alpha\beta}(\omega)=\sigma^{inter}_{\alpha\beta}(\omega)+\sigma^{intra}_{\alpha\beta}(\omega), \quad (3)$$

where $\sigma^{inter}_{\alpha\beta}(\omega)$ and $\sigma^{intra}_{\alpha\beta}(\omega)$ are the so-called inter- and intraband contributions, respectively. For the diagonal tensor components, both terms are important and should be considered simultaneously. The intraband contribution to the off-diagonal optical conductivity is very small and usually neglected in the case of magnetically ordered materials. For nonmagnetic metals (which have zero spontaneous exchange splitting), the spin polarization induced by the external magnetic field available in the experiment is small, and the contributions of intra- and interband transitions to the off-

diagonal optical conductivity tensor component can become comparable. Therefore, the intraband term should be taken into account on the same footing as the interband one.

The usual way to incorporate the intraband contribution to the optical conductivity tensor is to use the Drude model.[33] The classical equation of motion for a free electron in a magnetic field, with a damping constant $\gamma_D=\tau_D^{-1}$, where τ_D is a phenomenological Drude electron relaxation time, gives the following expressions for the intraband contributions to the diagonal $\sigma_{xx}^D(\omega)$ and off-diagonal $\sigma_{xy}^D(\omega)$ part of the optical conductivity tensor:[31,32]

$$\sigma_{xx}^D(\omega)=\frac{\omega_p^2}{4\pi}\frac{(\gamma_D-i\omega)}{(\gamma_D-i\omega)^2+\omega_c^2}, \tag{4}$$

$$\sigma_{xy}^D(\omega)=\frac{\omega_p^2}{4\pi}\frac{\omega_c}{(\gamma_D-i\omega)^2+\omega_c^2}, \tag{5}$$

with $n=(m^*\omega_p^2/4\pi e^2)^{1/2}$ being the carrier concentration and ω_c being the cyclotron frequency

$$\omega_c=eH/m^*c, \tag{6}$$

where H is the applied magnetic field, e is the electron charge, $m^*=m(1+\lambda)$ is the effective mass of the carrier, renormalized in solids by the electron-phonon interaction constant λ, and ω_p is the plasma frequency.

To apply the formula (5), suitable values of the parameters are needed. As a first approximation, zero-frequency values taken from dc-transport measurements can be used. The $\sigma_{xx}^D(\omega)$ and $\sigma_{xy}^D(\omega)$ conductivities for $\omega=0$ are

$$\sigma_{xx}^D(0)=\frac{1}{\varrho}, \tag{7}$$

$$\sigma_{xy}^D(0)=-\frac{\varrho_H}{\varrho^2}, \tag{8}$$

where ϱ and ϱ_H are dc and Hall resistivity, respectively.[31,32]

On the other hand, from expressions (4) and (5) the following formulas for $\sigma_{xx}^D(0)$ and $\sigma_{xy}^D(0)$ can be obtained for $\gamma_D \gg \omega_c$:

$$\sigma_{xx}^D(0)=\frac{\omega_p^2}{4\pi}\frac{1}{\gamma_D}, \tag{9}$$

$$\sigma_{xy}^D(0)=\frac{\omega_p^2}{4\pi}\frac{\omega_c}{\gamma_D^2}. \tag{10}$$

From the comparison of the Eqs. (7) and (9) and Eqs. (8) and (10), the γ_D can be expressed as

$$\gamma_D=\frac{\varrho}{|\varrho_H|}\omega_c. \tag{11}$$

The details of the computational method used for the linear muffin-tin orbital (LMTO) calculations are described in our previous paper[26] and here we only mention a few aspects. The electronic structure of Pt was calculated self-consistently using the local spin-density approximation[34] (LSDA) and the fully relativistic spin-polarized (SPR) LMTO method[35–37] in the atomic-sphere approximation including the combined correction (ASA+CC).[35,38] The basis consisting of *s*, *p*, *d*, and *f* LMTO's was used. Core-charge densities were recalculated at every iteration of the self-consistency loop. The **k**-space integrations were performed with the improved tetrahedron method[39] and the charge self-consistency was achieved with 12 000 irreducible **k** points. The effect of an external magnetic field on the band structure can be accounted for by including in the Hamiltonian the sum of the Zeeman term

$$H_Z=\mu_B\boldsymbol{B}\cdot(\boldsymbol{l}+2\boldsymbol{s}), \tag{12}$$

which couples spin $\boldsymbol{s}$ and orbital $\boldsymbol{l}$ moments of an electron to the external magnetic field $\boldsymbol{B}$, and the term responsible for diamagnetic effects. However, the analysis of the Knight shift and susceptibility of Pt by Clogston *et al.*[40] shows that the van Vleck second-order orbital susceptibility, Pauli spin susceptibility of the *s* band, and the diamagnetic susceptibility sum to zero. Thus, the measured susceptibility should be equal to the Pauli susceptibility of the *d* band. In accordance with this observation, in the present work the band structure of paramagnetic Pt in an external magnetic field was calculated self-consistently with the matrix elements of only the spin-dependent part of the Zeeman term (12) included in the Hamiltonian matrix of the LMTO method at the variational step.

The optical conductivity of Pt has been computed from the energy band structure by means of the Kubo-Greenwood[41] linear-response expression:[42]

$$\sigma_{\alpha\beta}(\omega)=\frac{-ie^2}{m^2\hbar V_{uc}}\times\sum_{\mathbf{k}}\sum_{nn'}\frac{f(\epsilon_{n\mathbf{k}})-f(\epsilon_{n'\mathbf{k}})}{\omega_{nn'}(\mathbf{k})}\frac{\Pi_{n'n}^{\alpha}(\mathbf{k})\Pi_{nn'}^{\beta}(\mathbf{k})}{\omega-\omega_{nn'}(\mathbf{k})+i\gamma}, \tag{13}$$

where $f(\epsilon_{n\mathbf{k}})$ is the Fermi function, $\hbar\omega_{nn'}(\mathbf{k})\equiv\epsilon_{n\mathbf{k}}-\epsilon_{n'\mathbf{k}}$ is the energy difference of the Kohn-Sham energies, and γ is the lifetime parameter, which is included to describe the finite lifetime of the excited Bloch electron states. The $\Pi_{nn'}^{\alpha}$ are the dipole optical transition matrix elements, which in a fully relativistic description are given by

$$\Pi_{nn'}(\mathbf{k})=m\langle\psi_{n\mathbf{k}}|c\boldsymbol{\alpha}|\psi_{n'\mathbf{k}}\rangle, \tag{14}$$

with $\psi_{n\mathbf{k}}$ being the four-component Bloch electron wave function. The combined correction terms were also taken into account in the optical matrix element calculations. A detailed description of the optical matrix elements in the Dirac representation is given in Ref. 11. Last, we mention that the absorptive part of the optical conductivity was calculated in a wide energy range and then the Kramers-Kronig transformation was used to calculate the dispersive parts of the optical conductivity from the absorptive ones. For the interband relaxation parameter we used the value $\gamma=0.5$ eV. The plasma frequency, ω_p in Eqs. (4) and (5) was calculated using the expression

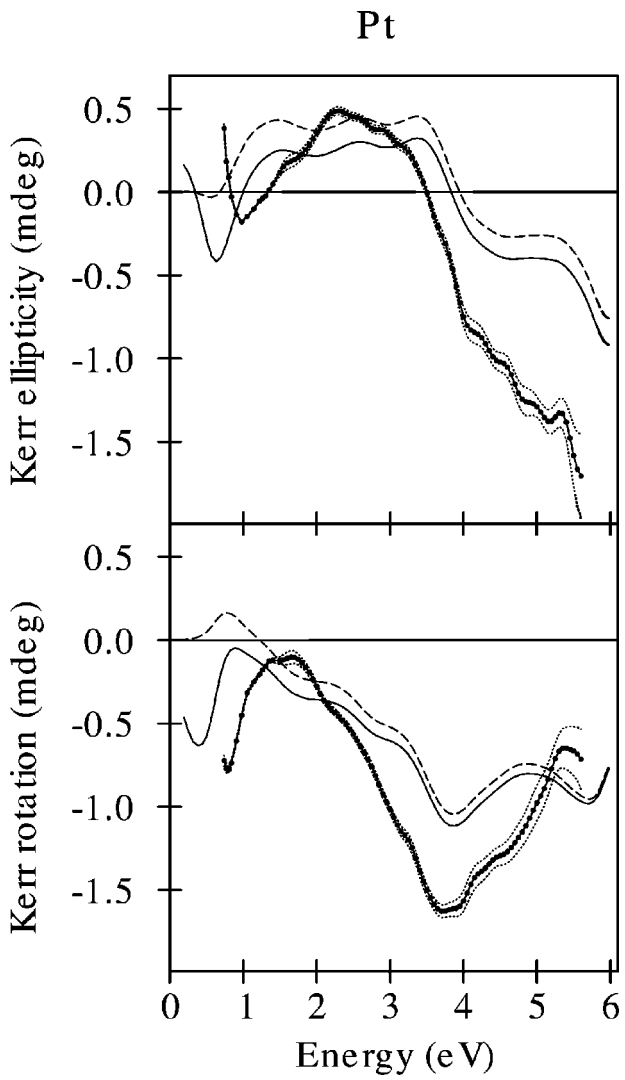

FIG. 1. Comparison between the experimental polar Kerr rotation and ellipticity spectra (circles), with error bars indicated by dotted lines, of fcc Pt metal film measured in the applied field of 1.5 T and the spectra calculated by the SPR LMTO method without intraband transitions (dashed lines) and with the intraband transitions included with $\gamma_D = 0.34$ eV (full lines).

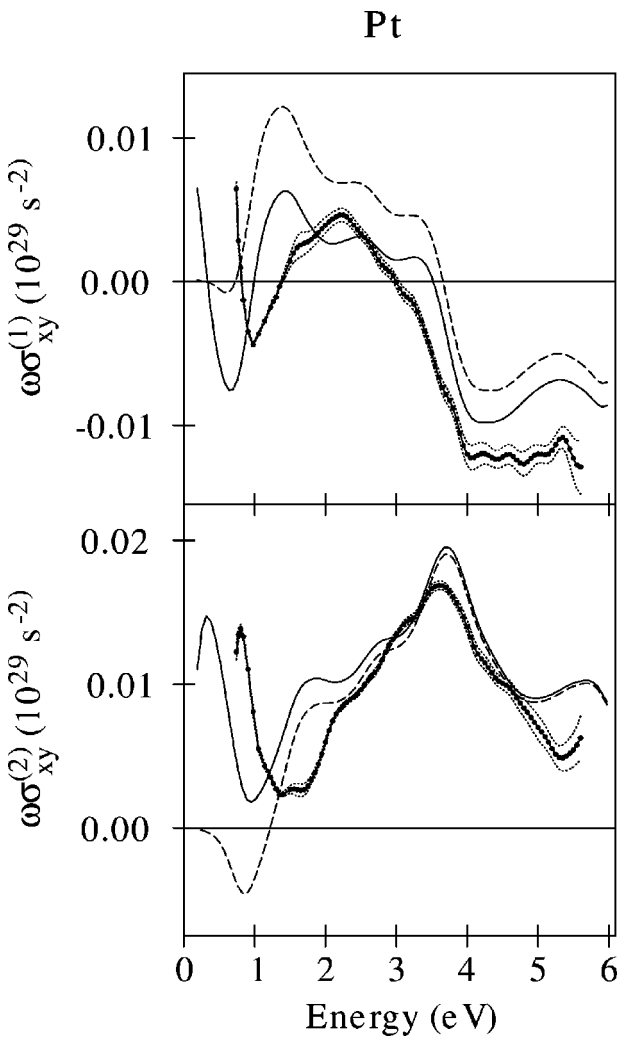

FIG. 2. Comparison between the experimental off-diagonal optical conductivity $\omega\sigma_{xy}$ spectra (circles), with error bars indicated by dotted lines, of fcc Pt metal film measured in the applied field of 1.5 T and the spectra calculated by the SPR LMTO method without intraband transitions (dashed lines) and with the intraband transitions included with $\gamma_D = 0.34$ eV (full lines).

$$(\omega_p)^2 \equiv \frac{4\pi e^2}{m^2 V_{uc}} \sum_{n\mathbf{k}} \delta(\epsilon_{n\mathbf{k}} - E_F) |\Pi_{nn}|^2, \qquad (15)$$

where E_F is the Fermi energy.

III. EXPERIMENTAL RESULTS AND COMPARISON WITH THEORY

Averaged experimental MOKE spectra of the paramagnetic Pt metal film measured in a magnetic field of 1.5 T (circles) are compared to the corresponding theoretically calculated spectra (dashed lines) in Fig. 1. The Kerr rotation and ellipticity in the ir and uv spectral ranges are of comparable magnitude and do not exceed the value of $\sim 2 \times 10^{-3}$ deg in a field of 1.5 T. The characteristic features of the measured Pt Kerr rotation spectrum are a broad maximum in the ir spectral range at ~ 1.5 eV and a prominent negative peak in the uv range at 3.8 eV. The essential points of the experimental Kerr ellipticity spectrum are the zero crossings at 1.5 eV and around 3.5 eV (which correspond to the peak positions in the Kerr rotation), with a broad positive structure between them and a negative shoulder at the energy of ~ 4 eV. A narrow negative peak is observed in the Kerr rotation at ~ 0.8 eV near the edge of the energy interval in which the measurements were performed, which coincides with the Kerr ellipticity zero-crossing at the same energy. We should mention that while the sensitivity of the experimental procedure used in the present work is generally within the 0.01–0.1 mdeg range (depending on the photon energy and corresponding photon shot noise), the variances (indicated in Fig. 1 by the dotted lines) increase significantly (up to ± 0.2 mdeg) at the high-energy edge of the measured energy interval.

The agreement between the experimental and calculated polar Kerr rotation spectrum in the vis-uv spectral range is good. The theoretical calculations reproduce the main peak at 3.8 eV and even the smooth shoulder visible in the experimental Kerr rotation spectrum at ~ 3 eV. For the Kerr el-

lipticity, a quantitative discrepancy between the theory and the experiment is somewhat larger, but the overall shape of the spectrum is reproduced well by the calculations. However, the low-energy part of the spectra below 1.5 eV exhibits considerable discrepancies. While the theoretical Kerr rotation forms a positive maximum around 1 eV and then goes smoothly to zero as the photon energy decreases, the experimental curve remains negative in the whole energy range and shows a sharp narrow minimum at ~ 0.8 eV. The same type of disagreement is seen also between the theoretical and experimental Kerr ellipticity spectra for which again below 1.5 eV the theoretical curve goes to zero, whereas the experimental curve forms the negative minimum and then increases abruptly towards the positive values after the zero crossing at 0.8 eV. It should be pointed out that the above-discussed experimental spectra were compared to the theoretical spectra calculated with neglect of the intraband contribution to the off-diagonal part of the optical conductivity. The importance of this contribution and its effect on the MOKE spectra of Pt will be discussed below.

The interpretation of the MOKE spectra in terms of electronic transitions is a nontrivial task because the complex Kerr rotation is a rather complicated function of both the diagonal and off-diagonal components of the optical conductivity tensor [Eq. (1)]. The off-diagonal part of the conductivity tensor of Pt obtained from the experimental MOKE spectra and the complex index of refraction (n and k) determined from the ellipsometry measurements are presented in Fig. 2. As seen from the comparison of Figs. 2 and 1 there is a close resemblance between the complex Kerr rotation spectra and the off-diagonal optical conductivity tensor components $\omega\sigma_{xy}^{(1)}$ and $\omega\sigma_{xy}^{(2)}$. This can be explained by the fact that in the considered energy range the optical constants n and k are essentially featureless functions of the photon energy, and all peculiarities of the Pt MOKE spectra are determined by the corresponding features of the σ_{xy} spectra (the measured n and k spectra agree well with those in Ref. 2). In the energy region above ~ 2 eV (see Fig. 2) the experimental $\omega\sigma_{xy}^{(2)}(\omega)$ spectrum agrees well with the calculated one both in the shape and the amplitude. In particular, the energy position and the magnitude of the peak at 3.8 eV are very well reproduced. On the other hand, the low-energy part of the spectrum below 2 eV exhibits considerable discrepancies. The same type of disagreement as in the case of Kerr ellipticity spectra is also seen between the theoretical and experimental spectra of $\omega\sigma_{xy}^{(1)}(\omega)$, where below 1.5 eV the theoretical curve gradually tends to zero, whereas the experimental curve crosses the zero level and tends to change abruptly towards the positive values. One of the possible reasons for the observed large discrepancy in the energy dependence of the $\omega\sigma_{xy}(\omega)$ in the ir energy range is the contribution from the intraband transitions to the off-diagonal conductivity that has not been included in the calculations of the theoretical spectra.

To study the influence of the intraband contribution on the MO properties of Pt the phenomenological Drude-like model has been adopted in the present work. To use the Drude model in the form of Eqs. (4) and (5) we need three parameters: the plasma frequency ω_p, the cyclotron frequency ω_c, and the damping constant γ_D. The first two parameters, $\omega_p = 7.32$ eV and $\omega_c = 1.02\times 10^{-4}$ eV, were calculated using

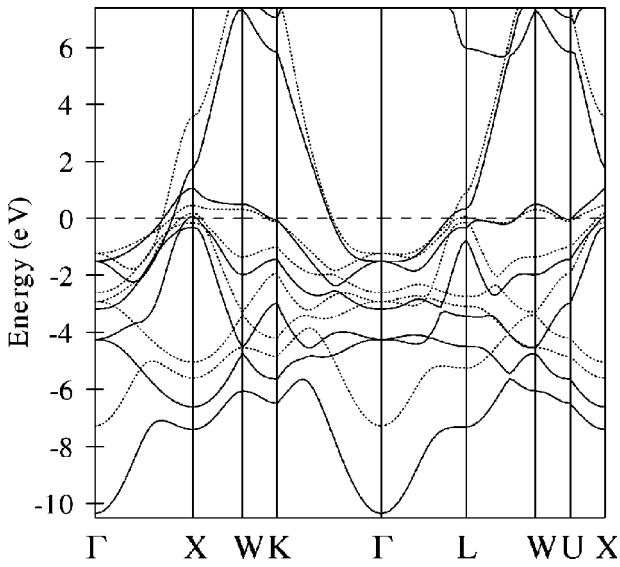

FIG. 3. Energy-band structure of fcc Pt (full lines) and Pd (dotted lines).

the Eqs. (15) and (6), respectively. To estimate the renormalized effective electron mass m^* we used the constant of the electron-phonon interaction $\lambda = 0.7$ calculated in the rigid MT approximation in Ref. 8. The inverse intraband Drude relaxation time γ_D can be estimated from the dc and Hall resistivity data using expression (11). Such an estimation using the values of $\varrho = 10.8\times 10^{-6}$ Ω cm and $\varrho_H = 3.3 \times 10^{-9}$ Ω cm (at 300 K in the magnetic field of 1.5 T) taken from Ref. 43 gives $\gamma_D = 0.34$ eV.

Adding the intraband contribution term to the off-diagonal conductivity with the value of the relaxation time parameter $\gamma_D = 0.34$ eV leads to the substantial improvement of the agreement between theoretical and experimental spectra, especially in the ir energy range (solid lines in Figs. 1 and 2). We should point out that the contribution of the intraband transitions $\sigma_{xy}^{D(2)}(\omega)$ to the absorptive part of the off-diagonal optical conductivity is proportional to $1/\omega^3$ for $\omega \gg \gamma_D$ and is important only in the ir energy range. As a consequence, this contribution determines the low-frequency behavior of the Kerr rotation spectrum, whereas in the vis-uv range its effect is relatively small. At the same time, $\sigma_{xy}^{(1)}(\omega)$ and the Kerr ellipticity are affected by the off-diagonal Drude term in the whole energy interval studied (Figs. 1 and 2) as $\sigma_{xy}^{D(1)}(\omega)$ decreases only as $1/\omega^2$ at high frequencies. In conclusion it can be stated that the energy dependence of the off-diagonal optical conductivity as well as the MOKE spectra of Pt are greatly affected by the contribution from the intraband optical transitions.

Although both the spectral shape and the magnitude of the experimental optical conductivity spectra are well reproduced by the LSDA calculations (Fig. 2), the position of the calculated prominent peak at 0.8 eV in $\sigma_{xy}^{(2)}(\omega)$ and corresponding structures in $\sigma_{xy}^{(1)}(\omega)$ are shifted to smaller energies as compared to the experimental spectra. One of the possible reasons is that due to the nonexact treatment of the electron exchange and correlations, the LSDA overestimates the d-band widths for transition metals of the end of the series.

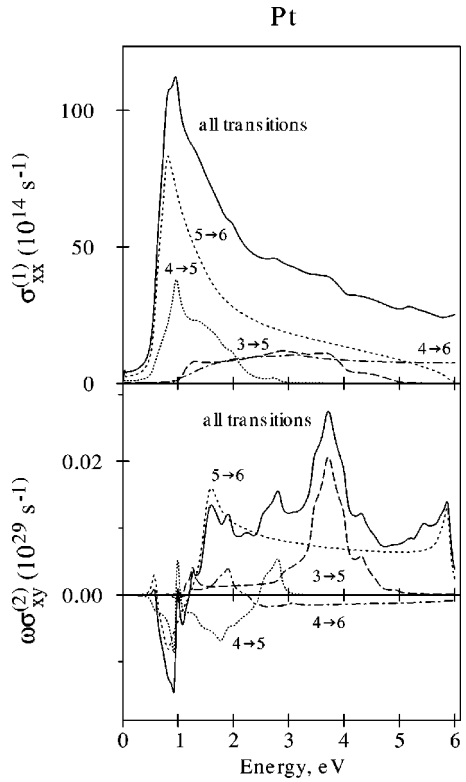

FIG. 4. Contributions of different interband transitions to the diagonal $\sigma_{xx}^{(1)}$ and off-diagonal $\sigma_{xy}^{(2)}$ spectra (solid lines) of fcc Pt in the magnetic field of 1.5 T: $3\rightarrow5$ (long-dashed lines), $5\rightarrow6$ (short-dashed), $4\rightarrow6$ (dashed-dotted), and $4\rightarrow5$ (dotted lines).

IV. ANALYSIS OF THE MAGNETO-OPTICAL TRANSITIONS IN Pt

To elucidate the microscopic origin of the MO properties of Pt metal in terms of electronic transitions, in the first step we consider its electronic structure in detail. The electronic structure underlying the optical transitions responsible for the MOKE spectra of Pd metal was studied in Ref. 30. To understand the cause of the observed differences in the resulting MOKE response of both metals, in the following discussion a direct comparison between the results for Pt and Pd will be performed. The calculated band structure of fcc Pt and Pd (included for comparison) is shown in Fig. 3. In the absence of magnetic field, due to time-reversal symmetry, all bands of Pt and Pd are at least twofold degenerate. The external magnetic field lifts the degeneracy. In the following analysis, to distinguish individual bands it will be convenient to keep the numeration of the bands by pairs, adding a subscript if necessary. Thus, for example, the ''transition $n\rightarrow m$'' means the sum over the four possible interband transitions between the initial pairs of bands $n_{1,2}$ and final pairs of bands $m_{1,2}$.

Although the energy-band structures of Pt and Pd (Fig. 3) are very similar, there are some distinctive differences in bandwidths and the energy positions of the bands (especially in X and L symmetry points near the Fermi level). It is mainly due to different spin-orbit splitting, slightly different lattice constants, and the difference in the spatial extent of $4d$ and $5d$ valence wave functions of Pd and Pt metals.

The small differences in the band positions lead to significant differences in the MO properties of two sister metals. Although the spin-orbit interaction in Pt is three times larger than that in Pd, the peak-to-peak amplitude of Kerr rotation in Pt is of comparable value with that of Pd. It is due to a notable difference in their paramagnetic susceptibility. The magnetic moments induced by the external magnetic field of 1.5 T are equal to $0.29\times10^{-3}\mu_B$ and $0.96\times10^{-3}\mu_B$ in Pt and Pd, respectively, as was estimated from paramagnetic susceptibility data (the values agree well with those obtained from the calculations).

A. The band-by-band decomposition

To identify the electronic interband transitions responsible for MO effects, the analysis of the spectral dependence of the optical conductivity tensor should be performed. The absorptive parts of the diagonal optical conductivity tensor element, $\sigma_{xx}^{(1)}$, and of the off-diagonal element, $\sigma_{xy}^{(2)}$, are directly connected via Eq. (13) to the microscopic interband optical transitions.

As the absorptive parts of the optical conductivity are additive quantities, to explain the microscopic origin of the MOKE activity of Pt in terms of individual electronic transitions, we performed the decomposition of the calculated $\sigma_{xx}^{(1)}$ and $\sigma_{xy}^{(2)}$ spectra into the contributions arising from separate interband transitions. (We neglect the intraband contributions for simplicity.) As one can see in Fig. 4, for photon energies up to 6 eV the $\sigma_{xx}^{(1)}$ of Pt is formed almost entirely by the transitions between 3, 4, 5 and 5, 6 bands. Having a look at the band structure (Fig. 3) one can see that the initial states for these transitions, bands $3_{1,2}$, $4_{1,2}$, and $5_{1,2}$, are rather narrow bands predominantly of d character, while the final states $6_{1,2}$ are wide free-electron-like s-p bands. The characteristic for the Pt intensive peak in $\sigma_{xx}^{(1)}$ around 1 eV is mainly determined by the $5\rightarrow6$ and the $4\rightarrow5$ transitions. The $4\rightarrow6$, $3\rightarrow6$, and $3\rightarrow5$ transitions beginning above 1 eV exhibit no pronounced structure in the 1 to 6 eV energy interval.

The characteristic features of $\sigma_{xy}^{(2)}$ of Pt are a negative peak at 1 eV, a positive structure in the range 2–3 eV, an intensive maximum at 3.8 eV, and a weaker positive peak at 5.5 eV. As it can be seen in Fig. 4, all the $\sigma_{xy}^{(2)}$ features, except the prominent peak at 3.8 eV, are mainly determined by the $5\rightarrow6$ and $4\rightarrow5$ transitions. The sharp peak at 3.8 eV, which can be considered as the ''fingerprint'' of the Pt MO response (see Fig. 2) is completely determined by the $3\rightarrow5$ transitions that overlap in the energy range, with almost constant contribution arising from the $5\rightarrow6$ transitions. It should be pointed out that the main features in the resulting $\sigma_{xx}^{(1)}$ and $\sigma_{xy}^{(2)}$ energy dependence of Pt are formed by different sets of interband transitions. The $\sigma_{xx}^{(1)}$ spectrum features are mainly determined by the $5\rightarrow6$ transitions with smaller contribution of the $4\rightarrow5$ transitions, whereas in the formation of $\sigma_{xy}^{(2)}$ spectra the $3\rightarrow5$ transitions play additionally an important role.

B. The k-space decomposition

To see how the interband transitions between the individual bands are located in the reciprocal space in both Pt and Pd, we performed the **k**-space decomposition of the interband transitions into transitions occurring in the vicinity

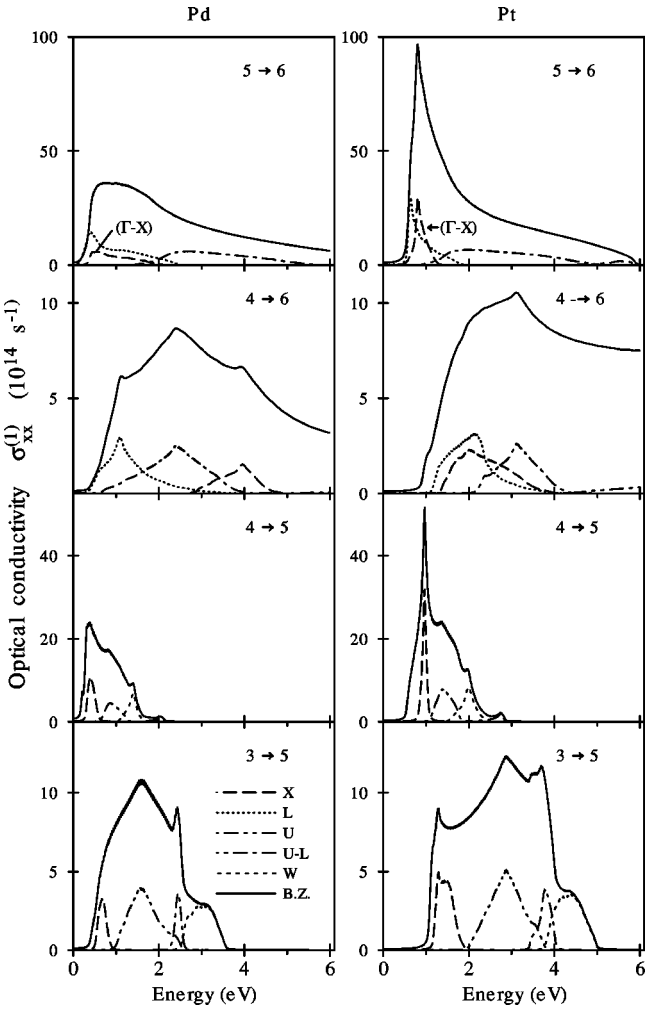

FIG. 5. Decomposition of the $\sigma_{xx}^{(1)}$ $n \rightarrow m$ interband transitions in Pt and Pd into transitions localized around different symmetry points in the BZ.

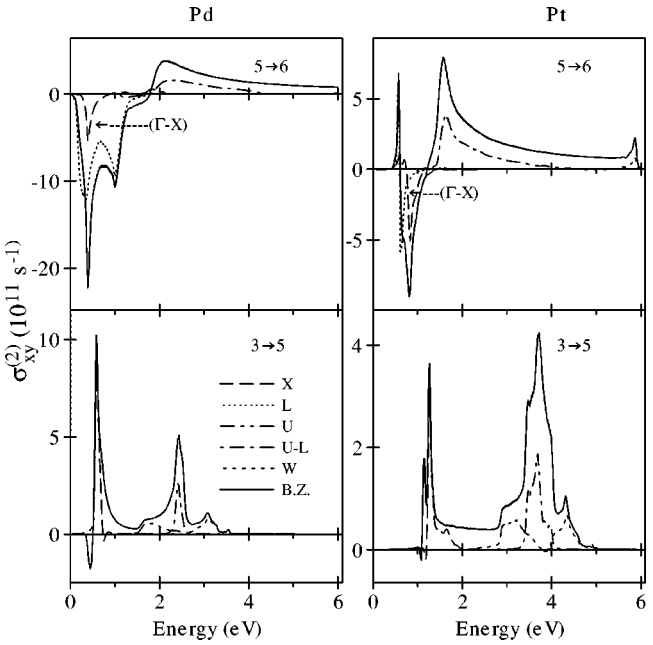

FIG. 6. Decomposition of the $\sigma_{xy}^{(2)}$ $n \rightarrow m$ interband transitions in Pt and Pd into transitions localized around different symmetry points in the BZ in a magnetic field of 1.5 T.

of the high-symmetry points of the Brillouin zone (BZ). For this aim we summed all transitions between the bands n and m in a cubic volume surrounding a given point with a cube edge equal to 0.125 of the Γ-X distance (it contains approximately 1.5% of a whole BZ volume). Although the results depend on the volume of the cube, one can identify the transitions essentially with these points and their nearest neighborhood.

Figures 5 and 6 illustrate the results of the decomposition. As it can be seen from Fig. 5, the main peak position of Pt arising from $4 \rightarrow 5$ transitions in $\sigma_{xx}^{(1)}$ at 1 eV is determined by the transitions near the X symmetry point. It should be pointed out that the spin-orbit interaction in solids splits some energy band states, e.g., $\Gamma_{25}' \rightarrow \Gamma_8^+ + \Gamma_7^+$, $X_5 \rightarrow X_6^+ + X_7^+$, and so on. In the central symmetry field model such a splitting is described by the spin-orbit parameter ζ_{nl}. This parameter is energy dependent in solids, and in cubic symmetry crystals can be estimated as the splitting of the top of the d energy band $\zeta_{nl}(E) \simeq E(X_7^+) - E(X_6^+)$.[44] So, the energy position of the main peak of the $4 \rightarrow 5$ optical transitions, which mainly occurs in the vicinity of the X point, gives direct information on the spin-orbit parameter $\zeta_{nl}(E)$ in the Pt and Pd metals (Fig. 5).

The final state for the $4 \rightarrow 5$ and $3 \rightarrow 5$ transitions is the same and, as a result, the transitions are located inside the same parts of the **k** space. The overall structure of both the $4 \rightarrow 5$ and $3 \rightarrow 5$ $\sigma_{xx}^{(1)}$ spectra is formed mainly by the transitions at the XUW edge plane of the BZ near X, U, and W for both metals. Due to the larger spin-orbit splitting, the corresponding features of the $3 \rightarrow 5$ and $4 \rightarrow 5$ transitions in Pt are shifted towards higher energy as compared to Pd. For both transitions there is also a contribution arising from the midpoint of the U-L line (the transition is very important for $\sigma_{xy}^{(2)}$ spectra; see Fig. 6). For the $3 \rightarrow 5$ transitions it manifests as sharp peaks at 2.5 and 3.8 eV in Pd and Pt, respectively. The same part of the **k** space is responsible for small peaks at 2 and 2.8 eV in $\sigma_{xx}^{(1)}$ for $4 \rightarrow 5$ transitions in Pd and Pt, respectively.

The $4 \rightarrow 6$ transitions for both metals are located in the same parts of the BZ, mainly near the L point in the Γ-U-L plane and near X. However, the energy positions of the transitions are significantly different in both metals. The maxima of $4 \rightarrow 6$ transitions in Pd occur near L and X at 1.2 eV and 4 eV, respectively, but both corresponding maxima in Pt occur at the same energy, 2 eV. Such a large difference is explained by significantly different energy positions of the 4 and 6 bands of Pd and Pt in the X and L points (Fig. 3) relative to the Fermi level.

The most intense $5 \rightarrow 6$ transitions in both metals arise from the same parts of BZ located near the L point along L-Γ and near the X point along the X-Γ direction. In the energy range from ~ 2 to 6 eV, the $5 \rightarrow 6$ transitions are located around the midpoint of the U-L line in both metals. As can be seen, for all the $5 \rightarrow 6$ transitions the initial states are located within the energy range of 0.5 eV below the Fermi level. The optical conductivity in Pt is larger than that in Pd. This, we believe, can be explained by the significantly larger spatial extent of the Pt $5d$ as compared to the Pd $4d$ wave

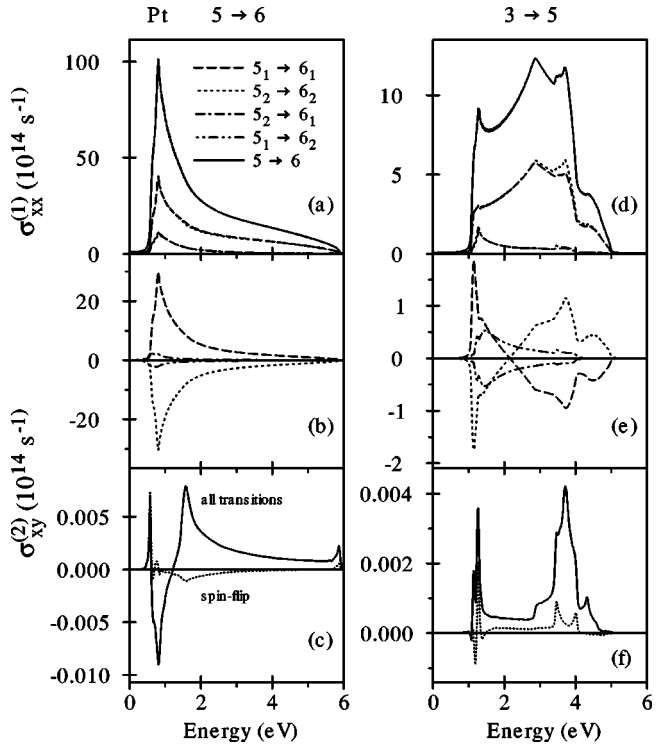

FIG. 7. Contributions of the individual transitions between the fifth and sixth pairs of the bands as well as between the third and fifth pairs to the $\sigma_{xx}^{(1)}$ and $\sigma_{xy}^{(2)}$ spectra of fcc Pt in a magnetic field of 1.5 T.

functions, which results in larger optical interband matrix elements in Pt in comparison with Pd ones.

Figure 6 shows the results of the **k**-space decomposition for the $5\rightarrow6$ and $3\rightarrow5$ transitions, responsible for the main features of the $\sigma_{xy}^{(2)}$ spectra of Pt and Pd. It should be pointed out that the magneto-optical transitions underlying the $\sigma_{xy}^{(2)}$ spectra of Pt and Pd are located in the same regions of the **k** space as the corresponding $\sigma_{xx}^{(1)}$ optical transitions discussed above. The $5\rightarrow6$ transitions in the energy range 1.5–5 eV for Pt and 2–6 eV for Pd, occurring mainly at the midpoint of the U-L line in the Γ-U-L plane, have more or less the same shape in both metals. On the other hand, the qualitative difference between $\sigma_{xy,5\rightarrow6}^{(2)}$ Pt and Pd is observed at the low-energy region. As mentioned before, the theoretical analysis shows that the $5\rightarrow6$ low-energy transitions, both in Pd and Pt, occur near the L point along the L-Γ direction and near the X point along the X-Γ direction. Due to the reconstruction of the fifth and sixth bands going from Pd to Pt, the $5\rightarrow6$ transitions around the L point manifest as an intense negative two-peak structure (at 0.4 and 1.0 eV) in Pd, whereas in Pt the corresponding structure forms a small positive peak at 0.5 eV and a negative one at 0.6 eV. The transitions that determine the characteristic shape of $\sigma_{xy}^{(2)}$ of Pt with the prominent peak at 3.8 eV (as discussed above, see Figs. 2 and 4) arise mainly from the $3\rightarrow5$ partial transitions, which are located near the U and W points and at the midpoint of the U-L line. For both metals, the low-energy part of the $3\rightarrow5$ MO transition is mainly determined by transitions at X. In conclusion, the individual interband $n\rightarrow m$ transitions arising from the same **k** points characterize essentially the same spectral shape in both metals. On the other hand, differences in band structure of Pd and Pt due to spin-orbit coupling strength and spatial extent of $4d$ and $5d$ wave functions result in different energy positions and intensities of the individual transitions that sum up to quite different overall optical and MO spectra in Pt and Pd.

C. Influence of the magnetic field and spin-orbit coupling on the interband transitions in Pt

To study the nature of the transitions responsible for the MO spectra features of Pt, we consider the structure of the selected interband transitions, $5\rightarrow6$ and $3\rightarrow5$, by considering their component transitions. In Fig. 7, the contributions to $\sigma_{xx}^{(1)}$ and $\sigma_{xy}^{(2)}$ of Pt arising from the four possible transitions between the pair of band states are shown, together with their sums. For the magnetic field used in the MOKE measurements, induced splitting of the bands is very small as compared to the bandwidths. In consequence, the joint densities of states for the transitions are similar, and the difference in the transitions' intensities is due to the corresponding matrix elements.

It should be recalled that, in the limit of zero spin-orbit coupling strength, the band indices 1 and 2 enumerate different projections of the electron spin, which is a good quantum number in this case, and the spin-flip $n_1\rightarrow m_2$ and $n_2\rightarrow m_1$ transitions are forbidden. The matrix elements of the spin-flip transitions depend on relative magnitudes of the spin-orbit splitting and crystal-field splitting and differ in different parts of the Brillouin zone.

As it is seen in Fig. 7, the spin-flip transitions have the largest intensities mainly in the ir spectral range. As it was shown above, in this energy region $3\rightarrow5$ transitions take place at X and $5\rightarrow6$ transitions near L in the Γ-L direction. For the spin-orbit coupling switched off, the 4 and 5 bands become degenerate along Γ-X and the 5 and 6 bands along the Γ-L direction. After switching on the spin-orbit interaction, the resulting band splitting is accompanied by a strong intermixing of the spin-up and spin-down states. On the other hand, the states at an arbitrary **k** point in the BZ, which are already split by the crystal field, do not undergo a further splitting.[45] As a result, enhanced spin-flip transitions occur mainly in the high-symmetry regions of **k** space.

Although for $\sigma_{xy}^{(2)}(\omega)$ the spin-flip transitions $5_1\rightarrow6_2$ and $5_2\rightarrow6_1$ are one order of magnitude smaller as compared to the direct spin-up and spin-down $5_1\rightarrow6_1$ and $5_2\rightarrow6_2$ transitions, the corresponding $3\rightarrow5$ transitions (spin-flip and direct ones) are of the same order of magnitude. As seen in Fig. 7, the amplitudes of the $3\rightarrow5$ component transitions are much smaller than the corresponding $5\rightarrow6$ transitions.

In the absence of the magnetic field, the bands are degenerate, and all the component spectra cancel exactly, leading to zero $\sigma_{xy}^{(2)}$ and MOKE. Due to the lifting of degeneracy caused by the magnetization, the component spectra are no longer equal and the resulting contribution of the $n\rightarrow m$ transition to $\sigma_{xy}^{(2)}(\omega)$ is given by a small-value difference of the two large quantities. Although the amplitudes of the individual transitions ($n_1\rightarrow m_2$, $n_2\rightarrow m_1$, $n_1\rightarrow m_1$ and $n_2\rightarrow m_2$) responsible for the absorption of the left and right polarized light are different for each $n\rightarrow m$ interband transition [Figs. 7(b) and (e)], they combine and produce spectra of the same order of magnitude but from three to four orders

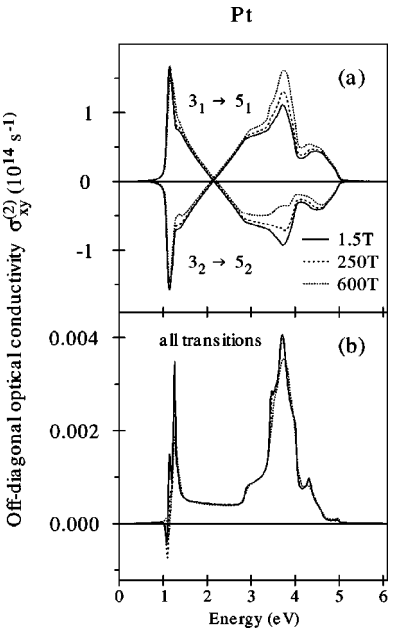

FIG. 8. The dependence of $\sigma^{(2)}_{xy,3_1\rightarrow 5_1}$ and $\sigma^{(2)}_{xy,3_2\rightarrow 5_2}$ components (a) and their sum, normalized vs the induced moment (see text) $\omega\sigma^{(2)}_{xy,3\rightarrow 5}$ (b) on the value of the magnetic field in fcc Pt.

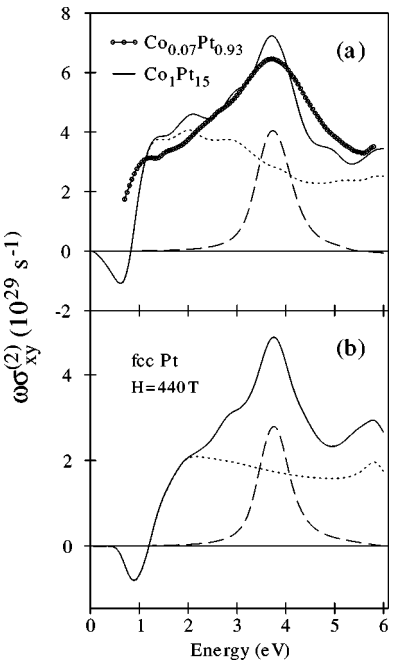

FIG. 9. Comparison between the experimental absorptive part of the off-diagonal optical conductivity $\omega\sigma_{xy}$ spectra of the $Co_{0.07}Pt_{0.93}$ diluted alloy [panel (a), circles, in arbitrary units] and the spectra calculated for the model Co_1Pt_{15} alloy (a) and fcc Pt in a magnetic field of 440 T (b) (solid lines). In the panels (a) and (b) dotted and dashed lines show the calculated contributions to spectra of Co_1Pt_{15} and fcc Pt coming from the transitions from shallow ($-1.8<E^{(i)}\leqslant 0$ eV, dotted lines) and deep ($-3.9<E^{(i)}\leqslant -3.1$ eV, dashed lines) initial states, respectively.

smaller than the component ones [at the magnetic field of 1.5 T, see solid lines in Figs. 7(c) and 7(f)]. As it will be shown later, when the magnetic field splitting ΔE of the bands is much smaller than the width of the *d* band, which occurs in the considered case of Pt, the resulting $\sigma^{(2)}_{xy,n\rightarrow m}$ spectra magnitude is proportional to the average bands' splitting. For both $3\rightarrow 5$ and $5\rightarrow 6$ transitions, the contribution of the spin-flip transitions themselves [shown by dotted lines in Figs. 7(c), 7(f)] to the total $\sigma^{(2)}_{xy}(\omega)$ remains relatively large for transitions occurring at high-symmetry points.

To study the dependence of the $\sigma^{(2)}_{xy}$ on the magnetic field, we performed the calculations gradually increasing the field value. It is known that in a wide range of magnetic field the nonlinear dependence of the induced magnetic moment on the field magnitude exists. It was verified that linear scaling in Pt up to a field of about 300 T holds, whereas in Pd the range of linearity is three times smaller[30] (this is because the magnetic susceptibility of Pt is about three times smaller as compared to Pd). In the ranges of the magnetic field indicated, the linearity between the $\sigma^{(2)}_{xy}$ amplitude and the value of the external magnetic field is preserved.

In Fig. 8(a) the influence of the magnetic field on the $\sigma^{(2)}_{xy,3\rightarrow 5}$ spectra is illustrated for the selected values of the external magnetic field. As can be seen, the calculated spectra for $\sigma^{(2)}_{xy,3_1\rightarrow 5_1}$ and $-\sigma^{(2)}_{xy,3_2\rightarrow 5_2}$ components change considerably when the magnetic field value increases, but the resulting spectra [Fig. 8(b)] are very close to each other. The resulting $\sigma^{(2)}_{xy,3\rightarrow 5}$ spectra have been normalized via a scaling down by a factor equal to the ratio of calculated magnetic moment to the moment obtained at a field of 1.5 T.

The dependences of the component $\sigma^{(2)}_{xy,n_2\rightarrow m_2}$ and $\sigma^{(2)}_{xy,n_1\rightarrow m_1}$ spectra and their sum on the magnitude of the external magnetic field in different energy regions are determined by the nature of the transition. For the transitions for which both the initial and final states do not cross the Fermi level, the induced band splitting results in a shift of the $\sigma^{(2)}_{xy,n_2\rightarrow m_2}$ spectra relative to $\sigma^{(2)}_{xy,n_1\rightarrow m_1}$ ones, and the resulting $\sigma^{(2)}_{xy}\sim(\partial\sigma^{(2)}_{xy,n_n\rightarrow m_n}/\partial E)H$.

On the other hand, when the band crosses the Fermi level at a given $\mathbf{k}$ of reciprocal space, the induced band splitting ΔE leads to changes of state occupations. The spin-up states become occupied and spin-down states unoccupied within a volume of $\Delta\mathbf{k}$ of BZ proportional to the splitting ΔE. For the transitions to (or from) such states, only transitions to the spin-down (or from the spin-up) states are allowed, and a strong linear dependence of the amplitude of the component transitions on ΔE arises. The contribution of these transitions to $\sigma^{(2)}_{xy}$ spectra is proportional to the $\sigma^{(2)}_{xy,n_n\rightarrow m_n}$ itself, and, as it can be easily shown, is of the form $\Delta\sigma^{(2)}_{xy}\sim[\sigma^{(2)}_{xy,n_n\rightarrow m_n}/\nabla_{\mathbf{k}}E(\mathbf{k})]H$. It can be seen that for a band crossing the Fermi level horizontally, the $\Delta\sigma^{(2)}_{xy}$ can add a very substantial contribution to the component spectra as well as the total spectra. This is the origin of the significant intensity of the $3\rightarrow 5$ transition at 3.8 eV and its behavior in the magnetic field. It was verified that the resulting $\sigma^{(2)}_{xy}$ spectrum magnitude scales with the induced magnetic moment and with the magnetic field as long as the proportionality between the band splitting and magnetic field holds.

D. Magneto-optical properties of Pt in dilute magnetic alloys

To show that the peak at $\sim$3.8 eV in the Kerr rotation spectrum of paramagnetic Pt is closely related to the peak

observed at the same energy in magnetic TM–Pt metal systems we present as an example in Fig. 9(a) the absorptive part of the $\omega\sigma_{xy}(\omega)$ spectrum for the dilute $Co_{0.07}Pt_{0.93}$ alloy. The spectrum was derived from the complex Kerr rotation spectra and ellipsometric data measured for the sputter-deposited disordered fcc $Co_{0.07}Pt_{0.93}$ alloy film.[46] Comparing the spectrum to the spectrum of paramagnetic Pt (Fig. 2) one can note that their overall shapes are strikingly similar. Marked differences between the $\omega\sigma_{xy}(\omega)$ spectrum of fcc Pt and $Co_{0.07}Pt_{0.93}$ alloy observed in the ir range arise in part due to the negligible contribution of the intraband transitions in the magnetic alloy. However, the position and shape of the prominent peak in uv range at 3.8 eV in both systems are the same. This leads to the conclusion that the MOKE response of Pt-rich alloys with the magnetic $3d$ metals in the uv range is mainly determined by MO properties of spin-polarized Pt, which is supported by the results of model calculations.

Figure 9(a) shows the calculated $\omega\sigma_{xy}(\omega)$ spectrum of an ordered Co_1Pt_{15} alloy ($Im3m$ space group symmetry) with the composition closest to the experimentally studied one. Although the experimental spectrum is less structured as compared to the theoretical spectrum owing to the broadening effects caused by the disordered structure of the sample, the spectral dependence of the theoretical optical conductivity agrees very well with the experiment [presented in arbitrary units in Fig. 9(a) to simplify shape comparison].

The theoretical spectrum of Co_1Pt_{15} alloy is to be compared with the $\omega\sigma_{xy}(\omega)$ spectrum of paramagnetic Pt [solid line in Fig. 9(b)] calculated for the external magnetic field of 440 T that is enough to induce the Pt magnetic moment of $0.085\mu_B$ close to the average Pt moment calculated for ferromagnetic Co_1Pt_{15} alloy. The comparison of the theoretical spectra reveals again their close similarity in the energy range 3–5 eV. Detailed analysis and the identification of the bands and transitions responsible for the main spectral features in TM–Pt compounds as a function of composition lead to a series of results the exhaustive presentation of which is beyond the scope of the present paper and will be given elsewhere.[47]

Here we restrict ourselves to performing the decomposition of both the alloy and Pt spectrum into the contributions from the interband transitions coming from the initial states lying in different energy ranges below the Fermi level to all final states. The dotted and dashed lines in Fig. 9 show the contribution to the $\omega\sigma_{xy}(\omega)$ spectra of Co_1Pt_{15} and strongly magnetized fcc Pt coming from the transitions from shallow ($-1.8<E^{(i)}\leqslant 0$ eV) and deep ($-3.9<E^{(i)}\leqslant -3.1$ eV) initial states, respectively. It should be noted that these two groups of transitions determine practically the whole resulting spectra of both Pt and the alloy. In Pt, the optical transitions from shallow and deep states are clearly identified as the transitions mainly from fifth to sixth and from third to fifth bands, respectively (see Fig. 4). Although in the Co_1Pt_{15} alloy the electronic band structure (not shown) changes due to hybridization with Co $3d$ states, the spectral shapes of the contribution from the both groups of transitions in Co_1Pt_{15} are closely related to those of fcc Pt [Figs. 9(a) and 9(b)]. However, the modification of the part of the spectrum formed by the transitions from the shallow states in the ir energy range due to the presence of $3d$ atoms is clearly seen for the Co_1Pt_{15} alloy. It can be supposed in advance that the differences between the spectra formed by the shallow states will become more pronounced with an increase of the $3d$ metal content. On the other hand, focusing our attention on the main spectral feature of the $\omega\sigma_{xy}(\omega)$ spectrum of Co-Pt compounds (i.e., the peak at 3.8 eV), we can state that the contribution of the transitions with the initial states lying in the range $-3.9<E^{(i)}\leqslant -3.1$ eV for the Co_1Pt_{15} alloy and Pt are basically the same. Moreover, it was verified that the final states for these transitions are located in the narrow energy range up to 0.3 eV above the Fermi level. We found that both groups of transitions are responsible for the $\omega\sigma_{xy}(\omega)$ spectrum in the case of the Fe_1Pt_{15} alloy.

The main features of the $\omega\sigma_{xy}(\omega)$ spectra in strongly dilute TM–Pt magnetic alloys and their close resemblance to the spectrum of Pt metal in external magnetic fields can be understood if we consider the hybridization effects of the Pt $5d$ and TM $3d$ states. In TM-Pt alloys with small TM content there is a large number of Pt atoms that have only a few TM nearest neighbors, and the electronic states well below the Fermi level are formed mainly by Pt $5d$ states. These states, which are the initial states for the interband transitions forming the peak at 3.8 eV in the MO spectra, are modified only weakly by the hybridization with TM $3d$ states but nevertheless acquire a large exchange splitting. On the other hand, TM $3d$ states contribute more strongly to the states in the vicinity of the Fermi level and their contribution manifests itself in the changes of the MO spectra in the ir range. In conclusion, it can be stated that although the microscopic mechanisms of Pt spin polarization in the Pt-rich magnetic alloys and Pt metal differ, the spectral dependence of the MO response in the uv range of both systems is basically the same.

V. CONCLUSIONS

The magneto-optical response of the paramagnetic fcc Pt metal film measured in an external magnetic field of 1.5 T over the photon energy range $0.74\leqslant\hbar\omega\leqslant 5.6$ eV is presented. The band-structure and MOKE spectra calculations of paramagnetic Pt have been performed by the spin-polarized relativistic LMTO method within spin-density-functional theory, with the term $2\mu_B\mathbf{B}\cdot\mathbf{s}$ added to the Hamiltonian that couples spin of the electron to the external magnetic field.

It was shown that the frequency-dependent behavior of the off-diagonal optical conductivity is greatly affected by intraband optical transition contribution. If the influence of the intraband transitions on the absorptive part of the optical conductivity tensor $\sigma_{xy}^{(2)}(\omega)$ manifests mainly in the ir energy range from 0 to 1.5 eV, the dispersive part of the optical conductivity tensor $\sigma_{xy}^{(1)}(\omega)$ is affected by the intraband transitions in the wide energy interval studied. The calculations reproduce the experimentally observed Pt MOKE spectra in a very satisfactory way and explain their microscopic origin when the intraband and interband transitions are included simultaneously.

The band-by-band and the **k**-space decomposition of the fcc Pt and Pd MO spectra have been performed and the transitions responsible for the prominent structures in the spectra identified. The main role of the transitions from the states in the vicinity of the Fermi level in the formation of Pt MOKE

spectra is found. The dominant contribution which determines the characteristic shape of the $\sigma_{xy}^{(2)}$ spectrum of Pt with the prominent peak at 3.8 eV mostly comes from the $3\rightarrow5$ transitions at the edge of the BZ, namely, the middle point on the *U-L* direction and the *W* and *U* symmetry points. It was shown that the individual interband $n\rightarrow n'$ transitions in Pt and Pd metals are localized essentially around the same **k** points of the BZ and have the very close shape. The individual behavior of the resulting optical and MO response of the Pt and Pd metals comes from the difference in their spin-orbit coupling strength and spatial extent of $4d$ and $5d$ wave functions that result in different energy positions and intensities of the individual transitions that sum up to quite different overall optical and MO spectra. Comparative analysis of the off-diagonal optical conductivities in Pt and Pd clearly demonstrates that MO spectroscopy is a very sensitive method to investigate minor differences in the electronic structure of solids. It has been found and explained in terms of the band splitting that the proportionality between the magnetization and the magnitude of the Pt MOKE spectra holds in the wide tested range of the external magnetic fields. The correlations between the pure Pt MO spectrum and that of TM–Pt systems were found. It was shown that in the Pt-rich magnetic alloys the characteristic for the systems, strong enhancement of the MOKE spectra in uv range, can be considered as coming mainly from the spin-polarized Pt and the resulting spectral dependence of the underlying optical transitions depends only weakly on the source of Pt magnetization.

ACKNOWLEDGMENTS

V.N.A. gratefully acknowledges the hospitality during his stay at the Institute of Experimental Physics, University of Bialystok. This work was supported by the Polish State Committee for Scientific Research (KBN) under Contract No. 2 P03B 113 11.

*To whom any correspondence should be addressed; email address: ubaluba@venus.uwb.edu.pl

†Permanent address: Institute of Metal Physics, 36 Vernadskii Street, 252142 Kiev, Ukraine.

[1] J.R. Ketterson and L.H. Windmiller, Phys. Rev. Lett. **20**, 321 (1968); Phys. Rev. B **2**, 4814 (1970); D.H. Dye, J.B. Ketterson, and G.W. Grabtree, J. Low Temp. Phys. **30**, 813 (1978).

[2] J.H. Weaver, C. Krafka, D.W. Lynch, and E.E. Koch, *Optical Properties of Metals in Physics Data* (Fachinformationszentrum, Karlsruhe, 1981); J.H. Weaver, Phys. Rev. B **11**, 1416 (1975); M.M. Kirillova, L.V. Nomerovannaya, and M.M. Noskov, Fiz. Met. Metalloved. **34**, 60 (1972).

[3] V.V. Nemoshkalenko, Vl.N. Antonov, V.N. Antonov, W. John, H. Wonn, and P. Ziesche, Phys. Status Solidi B **111**, 11 (1982) (and references therein).

[4] N.V. Smith, Phys. Rev. B **9**, 1365 (1974); E.E. Krasovskii, A.N. Yaresko, and V.N. Antonov, J. Electron Spectrosc. Relat. Phenom. **68**, 157 (1994).

[5] O.K. Andersen and A.R. Mackintosh, Solid State Commun. **6**, 285 (1968); O.K. Andersen, Phys. Rev. B **2**, 883 (1970); N.E. Christensen, J. Phys.: Metal Phys. **8**, L.51 (1978); V.V. Nemoshkalenko, Vl.N. Antonov, and V.N. Antonov, Phys. Status Solidi B **99**, 471 (1980).

[6] F.Y. Fradin, D.D. Koelling, A.J. Freeman, and T.J. Watson-Yang, Phys. Rev. B **12**, 5570 (1975); V.Yu. Milman, T.A. Grischenko, K.L. Evlashina, A.V. Zhalko-Titarenko, V.N. Antonov, and V.V. Nemoshkalenko, J. Phys. Chem. Solids **53**, 565 (1992).

[7] V.N. Antonov, V.Yu. Milman, V.V. Nemoshkalenko, and A.V. Zhalko-Titarenko, Z. Phys. B: Condens. Matter **79**, 223 (1990); **79**, 233 (1990).

[8] D. Glützel, D. Ratner, and G.R. Schober, Z. Phys. B: Condens. Matter **35**, 317 (1979); W. John, V.V. Nemoshkalenko, V.N. Antonov, and Vl.N. Antonov, Phys. Status Solidi B **121**, 233 (1984); V.N. Antonov, Solid State Commun. **51**, 723 (1984); A.V. Zhalko-Titarenko, M.L. Evlashina, V.V. Nemoshkalenko, and V.N. Antonov, Phys. Status Solidi B **175**, 389 (1993).

[9] C. Schober, G. Kurz, H. Wonn, V.V. Nemoshkalenko, and V.N. Antonov, Phys. Status Solidi B **136**, 233 (1986); C. Schober and V.N. Antonov, *ibid.* **143**, K31 (1987); G.E. Grechnev, N.V. Savchenko, V.N. Antonov, A.V. Zhalko-Titarenko, M.I.G. Lee, and J.M. Perz, Fiz. Nizk. Temp. **13**, 1219 (1987) [Low Temp. Phys. **13**, 689 (1987)].

[10] M.M. Kirillova, L.V. Nomerovannaya, V.G. Topolsky, and V.P. Shirokosky, Fiz. Met. Metalloved. **52**, 530 (1981) (in Russian).

[11] V.N. Antonov, A.I. Bagljuk, A.Ya. Perlov, V.V. Nemoshkalenko, Vl.N. Antonov, O.K. Andersen, and O. Jepsen, Fiz. Nizk. Temp. **19**, 689 (1993) [Low Temp. Phys. **19**, 494 (1993)].

[12] V.N. Antonov, A.V. Zhalko-Titarenko, V.Yu. Milman, A. Khotkevich, and S.N. Krainyukov, J. Phys.: Condens. Matter **3**, 6523 (1991); S.N. Krainyukov, A. Khotkevich, I.K. Yanson, A.V. Zhalko-Titarenko, V.N. Antonov, and V.V. Nemoshkalenko, Fiz. Nizk. Temp. **14**, 235 (1988) [Low Temp. Phys. **14**, 127 (1988)].

[13] D. Weller, W. Reim, K. Spörl, and H. Brändle, J. Magn. Magn. Mater. **93**, 183 (1991); K. Sato, H. Ikekame, Y. Tosaka, K. Tsuzukiyama, Y. Togami, and M. Fujisawa, *ibid.* **126**, 572 (1993).

[14] K. Sato, H. Ikekame, Y. Tosaka, and S.-C. Shin, J. Magn. Magn. Mater. **126**, 553 (1993); S. Uba, L. Uba, and R. Gontarz, IEEE Trans. Magn. **MAG-30**, 806 (1994); S. Uba, L. Uba, A.N. Yaresko, A.Ya. Perlov, V.N. Antonov, and R. Gontarz, J. Phys.: Condens. Matter **10**, 447 (1998).

[15] C.-J. Lin, G.L. Gorman, C.H. Lee, R.F.C. Farrow, E.E. Marinero, H.V. Do, H. Notarys, and C.J. Chien, J. Magn. Magn. Mater. **93**, 194 (1991); K. Spörl and D. Weller, *ibid.* **93**, 379 (1991).

[16] E.E. Fullerton, D. Stoeffler, K. Ounadjela, B. Heinrich, Z. Celinski, and J.A.C. Bland, Phys. Rev. B **51**, 6364 (1995); J. Vogel, A. Fontaine, V. Cros, F. Petroff, J.-P. Kappler, G. Krill, A. Rogalev, and J. Goulon, *ibid.* **55**, 3663 (1997); O. Rader, E. Vescovo, J. Redinger, S. Blügel, C. Carbone, W. Eberthardt, and W. Gudat, Phys. Rev. Lett. **72**, 2247 (1994).

[17] W.B. Zeper, F.J.A.M. Greidanus, P.F. Carcia, and C.R. Fincher, J. Appl. Phys. **65**, 4971 (1989); H. Brändle, D. Weller, J.C. Scott, S.S.P. Parkin, and C.-J. Lin, IEEE Trans. Magn. **MAG-28**, 2967 (1992); K. Sato, H. Hongu, H. Ikekame, J. Watanabe, K. Tsuzukiyama, Y. Togami, M. Fujisawa, and T. Fukazawa, Jpn. J. Appl. Phys., Part 1 **31**, 3603 (1992); Š. Višňovský, M. Nyvlt, V. Parizek, P. Kielar, V. Prosser, and R. Krishnan, IEEE Trans. Magn. **MAG-29**, 3390 (1993); G. Armelles, D. Weller, B. Rellinghaus, R.F.C. Farrow, and M.F. Toney, *ibid.* **MAG-33**,

3220 (1994); E.T. Kulatov, Yu.A. Uspenskii, and S.V. Halilov, J. Magn. Magn. Mater. **163**, 331 (1996); R.J. Lange, S.J. Lee, D.W. Lynch, P.C. Canfield, B.N. Harmon, and S. Zollner, Phys. Rev. B **58**, 351 (1998).

[18] R.M. Bozorth, P.A. Wolff, D.D. Davis, V.B. Compton, and J.H. Wernick, Phys. Rev. **122**, 1157 (1961); J.W. Cable, E.O. Wollan, and W.C. Koehler, Phys. Rev. **138**, A755 (1965).

[19] G.R. Harp, D. Weller, T.A. Rabedeau, R.F.C. Farrow, and M.F. Toney, Phys. Rev. Lett. **71**, 2493 (1993).

[20] S. Uba, L. Uba, A.N. Yaresko, A.Ya. Perlov, V.N. Antonov, and R. Gontarz, Phys. Rev. B **57**, 1534 (1998).

[21] D. Weller, J. Sticht, G.R. Harp, R.F.C. Farrow, R.F. Marks, and H. Brändle, in *Magnetic Ultrathin Films-Multilayers and Surfaces, Interfaces and Characterization*, edited by B.T. Jonker, S.A. Chambers, R.F. C. Farrow, C. Chappert, R. Clarke, W.J.M. de Jonge, T. Egami, P. Grünberg, K.M. Krishnan, E.E. Marinero, C. Rau, and S. Tsunashima, MRS Symposia Proceedings No. 313 (Materials Research Society, Pittsburgh, 1993), p. 501.

[22] P.M. Oppeneer, V.N. Antonov, T. Kraft, H. Eschrig, A.N. Yaresko, and A.Ya. Perlov, Solid State Commun. **94**, 255 (1995).

[23] P.M. Oppeneer, V.N. Antonov, T. Kraft, H. Eschrig, A.N. Yaresko, and A.Ya. Perlov, J. Phys.: Condens. Matter **8**, 5769 (1996).

[24] S. Uba, L. Uba, R. Gontarz, V.N. Antonov, A.Ya. Perlov, and A.N. Yaresko, J. Magn. Magn. Mater. **140-144**, 575 (1995).

[25] G.Y. Guo and H. Ebert, Phys. Rev. B **51**, 12 633 (1995).

[26] S. Uba, L. Uba, A.N. Yaresko, A.Ya. Perlov, V.N. Antonov, and R. Gontarz, Phys. Rev. B **53**, 6526 (1996).

[27] G.Y. Guo and H. Ebert, J. Magn. Magn. Mater. **156**, 173 (1996).

[28] L. Uba, S. Uba, A.N. Yaresko, A.Ya. Perlov, V.N. Antonov, and R. Gontarz, J. Magn. Magn. Mater. **193**, 159 (1999).

[29] P.M. Oppeneer and V.N. Antonov, in *Energy-Band Theory of the Magneto-Optical Kerr Effect of Selected Ferromagnetic Materials*, in *Spin-Orbit Influenced Spectroscopies*, edited by H. Ebert and G. Schütz (Springer, Heidelberg, 1996), p. 29–47.

[30] A.N. Yaresko, L. Uba, S. Uba, A.Ya. Perlov, R. Gontarz, and V.N. Antonov, Phys. Rev. B **58**, 7648 (1998).

[31] W. Reim and J. Schoenes, in *Ferromagnetic Materials*, edited by E.P. Wohlfarth and K.H.J. Buschow (North-Holland, Amsterdam, 1990), Vol. 5, p. 133.

[32] J. Schoenes, in *Materials Science and Technology*, Vol. 3A: *Electronic and Magnetic Properties of Metals and Ceramics* (volume editor: K.H.J. Buschow), edited by R.W. Cahn, P. Haasen and E.J. Kramer (Verlag Chemie, Weinheim, 1992), p. 147.

[33] H.S. Bennet and E.A. Stern, Phys. Rev. **137**, A448 (1965).

[34] U. von Barth and L. Hedin, J. Phys. C **5**, 1629 (1972).

[35] O.K. Andersen, Phys. Rev. B **12**, 3060 (1975).

[36] V.V. Nemoshkalenko, A.E. Krasovskii, V.N. Antonov, Vl.N. Antonov, U. Fleck, H. Wonn, and P. Ziesche, Phys. Status Solidi B **120**, 283 (1983).

[37] V.N. Antonov, A.Ya. Perlov, A.P. Shpak, and A.N. Yaresko, J. Magn. Magn. Mater. **146**, 205 (1995).

[38] V.V. Nemoshkalenko and V.N. Antonov, *Computational Methods in Solid State Physics* (Gordon and Breach, London, 1998).

[39] P.E. Blöchl, O. Jepsen, and O.K. Andersen, Phys. Rev. B **49**, 16 223 (1994).

[40] A.M. Clogston, V. Jaccarino, and Y. Yafet, Phys. Rev. **4**, A650 (1964).

[41] J. Kubo, J. Phys. Soc. Jpn. **12**, 570 (1957).

[42] C.S. Wang and J. Callaway, Phys. Rev. B **9**, 4897 (1974).

[43] V. Frank, Appl. Sci. Res., Sect. B **B7**, 41 (1958).

[44] N.E. Christensen and B.O. Seraphin, Solid State Commun. **8**, 1221 (1970).

[45] J.M. Ziman, *Principles of the Theory of Solids* (Cambridge University Press, London, 1972).

[46] The amplitude of the Kerr rotation of the magnetic systems scales by the magnetization value and decreases with temperature acordingly to the Brillouin function. The complex Kerr rotation spectra of the $Co_{0.07}Pt_{0.93}$ film were measured at temperature of 290 K that is in the range close to the sample ordering temperature. The experimental spectrum magnitude in Fig. 9(a) is presented in arbitrary units because of the uncertainty in the determination of the sample Curie temperature. It should be noted that the ferromagnetic state of the alloy under study has been confirmed by the hysteresis loop measurement.

[47] L. Uba, S. Uba, V.N. Antonov, A.N. Yaresko, and R. Gontarz (unpublished).